Nuclear Materials and Energy 24 (2020) 100752

Contents lists available at ScienceDirect

Nuclear Materials and Energy

journal homepage: www.elsevier.com/locate/nme

Tungsten nitride as tritium permeation barrier

A. Houben[a,*], M. Rasiński[a], L. Gao[b], Ch. Linsmeier[a]

[a] Forschungszentrum Jülich GmbH, Institut für Energie- und Klimaforschung – Plasmaphysik, Partner of the Trilateral Euregio Cluster (TEC), 52425 Jülich, Germany
[b] Max-Planck-Institut für Plasmaphysik, Boltzmannstr. 2, 85748 Garching, Germany

ARTICLE INFO

Keywords:
Deuterium gas driven permeation
Tritium permeation barriers
RAFM steel/Eurofer97
Tungsten nitride
Layer permeability calculation

ABSTRACT

The development and application of robust tritium permeation barrier coatings is crucial for a safe and economic fusion reactor operation. Three different tungsten and tungsten nitride layers on Eurofer97 substrates were investigated by deuterium permeation measurements and compared. The microstructure and crystal structure was characterized before and after permeation measurements. The layer permeability is independent of the layer thickness and substrate of the sample. For a reliable comparison of different tritium permeation barrier coatings, the layer permeability of each layer was calculated. With this layer permeability, the permeation flux through potential fusion device components can be estimated. As examples, the permeation flux through a 0.5 cm thick steel component can be reduced by two orders of magnitude by a 2 μm thick WN layer and nearly four orders of magnitude by a 2 μm non-cracked tungsten layer.

1. Introduction

In order to reduce fuel loss and due to safety issues, tritium accumulation into fusion reactor walls and permeation through walls have to be prevented. Therefore, the development of tritium permeation barrier (TPB) coatings is crucial for a safe and economic fusion reactor operation. Ceramics, such as metal oxides, carbides and nitrides, were identified as high temperature resistant materials with a low hydrogen permeation [1]. During the last decades, the hydrogen permeation through various materials was measured and compared. Due to the strong dependence of the permeation on the microstructure of the TPB coating, the obtained results can vary widely. In order to understand and predict the hydrogen permeation process through barrier coatings, a detailed phase and microstructure analysis is important [2]. The thermal stability of TPB layers is of high importance as well, since cracks in the coating can act as shortcuts to the substrate and therefore cracks reduce the permeation reduction properties of the layer.

Tungsten is foreseen as divertor and first wall material in fusion devices, such as ITER. Due to the fact that the plasma has to be cooled at the plasma edge by impurities, nitrogen was successfully tested as a seeding gas in ASDEX Upgrade and JET [3,4]. By interaction of nitrogen with tungsten in the first wall or divertor, tungsten nitride phases will be formed [5]. The interaction with hydrogen of this tungsten nitride phases was studied and a lower hydrogen diffusion in tungsten nitride compared to pure tungsten was found [6,7]. Due to this observation, the deuterium permeability of tungsten nitride (WN) coatings is investigated in order to study the possible application of tungsten nitride as a TPB. In order to obtain an overview of the reduction effect of W and WN as TPB coatings, three different W and WN layers were produced by magnetron sputter deposition on Eurofer97 steel substrates, analyzed and compared.

2. Materials and methods

The reduced activation ferritic martensitic Eurofer97 steel substrates (disk shape with a diameter of 25 mm and a thickness of 0.3 mm) were mirror polished before layer deposition in the magnetron device. Three different layer systems were studied: a) a pure tungsten layer on a Eurofer97 substrate (named Eu97_W); b) a WN layer on a Eurofer97 substrate (named Eu97_WN); c) a WN layer on a Eurofer97 substrate which has a tungsten layer on top of the WN layer (named Eu97_WNW). These samples are compared with each other and to the bare Eurofer97 (named Eu97) substrate studied in [8]. The pure tungsten layers were deposited in DC-mode of the magnetron with an Ar plasma, whereas the WN layers were deposited in the reactive RF-mode of the magnetron with an Ar/N_2 plasma. The sputter target was in all cases pure tungsten. Details of the WN layer deposition can be found in [7]. After deposition, the samples were annealed in vacuum or deuterium at 550 °C in order to obtain stable crystal phases and to reduce the hydrogen content in the samples, since the natural hydrogen content could influence hydrogen isotope signals in the permeation measurements. Furthermore, the thermal stability was tested by this pre-

* Corresponding author.
E-mail address: an.houben@fz-juelich.de (A. Houben).

https://doi.org/10.1016/j.nme.2020.100752
Received 30 January 2020; Received in revised form 27 April 2020; Accepted 28 April 2020
Available online 11 May 2020

annealing. Before and after permeation measurements, the microstructure was investigated by scanning electron microscopy (SEM) on a cross section prepared by a focused ion beam (FIB) with a Zeiss Crossbeam 540 device. The crystal structure was studied by X-ray diffraction (XRD) with a Bruker Discovery diffraction device with Cu-radiation in Bragg-Brentano geometry. The deuterium gas-driven permeation was measured varying both pressure (25 mbar to 800 mbar) and temperature (300 °C to 550 °C). Each temperature step was measured twice (up-measurements from 300 °C to 550 °C and afterwards down-measurements from 550 °C to 300 °C) in order to investigate sample changes during measurement. If the sample state do not changed during measurement, e.g. due to oxidation of the sample surface or crack propagation in the layer, the measured values of the up- and down-measurements are identical for each temperature and pressure step. This confirms the good repeatability of the measurements in this device. The base pressure in the low and high pressure volumes was in the 10^{-9} mbar range. The deuterium permeation flux was measured in the low pressure volume by a quadrupole mass spectrometer (Pfeiffer Prisma Plus). The signal of the mass spectrometer was calibrated by four deuterium calibration leaks (LACO). Details of the setup and the measurement procedure can be found in [9,8].

3. Data analysis

The measured deuterium permeation flux is dependent on the diffusion and solubility of deuterium in the sample bulk and on surface effects. In the diffusion-limited regime, in which the surface processes are quick compared to the diffusion through the sample, the permeation flux can be expressed by:

$$J_P = \frac{P_0 \sqrt{p}}{d} e^{\frac{-E_P}{RT}} \quad (1)$$

wherein d is the thickness of the sample, P_0 and E_P the permeability constant and energy, respectively, p the applied deuterium pressure, T the sample temperature and R the ideal gas constant. With the permeability constant and activation energy, the temperature dependence of the permeability P of a material can be expressed by:

$$P = P_0 \cdot e^{\frac{-E_P}{RT}} \quad (2)$$

In a polycrystalline and non-defect free sample, the effective permeability is measured. In general, compared to the lattice permeability, which could be measured on a defect free and single crystalline sample, the effective permeability is higher. From the temperature dependent measurement, the permeability constant and the activation energy can be obtained by an Arrhenius plot.

The permeation reduction factor (PRF) is often used to compare different TPB and can be obtained by measuring the permeation flux through a coated sample and a bare reference substrate sample. The PRF value is defined by the permeation flux of the bare substrate divided by the permeation flux of a coated substrate at the same sample temperature and applied deuterium pressure. Since the PRF is strongly related to the permeability of the used substrate and the TPB layer thickness is not included in the PRF value, a comparison of measurements of the same TPB material performed by different research groups or of TPB layers to other substrate materials is complex by using only the PRF value. In order to enable a more reliable comparison, the layer permeability P_{lay} is calculated by

$$P_{lay} = \frac{d_{lay}}{\frac{d_{tot}}{P_{tot}} - \frac{d_{sub}}{P_{sub}}} \quad (3)$$

with the thickness of the layer d_{lay}, the thickness and permeability of the substrate d_{sub} and P_{sub} and the thickness and permeability of the layered substrate d_{tot} and P_{tot}, respectively. For details of the layer permeability calculation please refer to [10]. With the layer permeability, the permeability of the TPB layer can easily be compared to other TPB coatings and substrate materials. Furthermore, the permeation flux through potential fusion device components can be estimated.

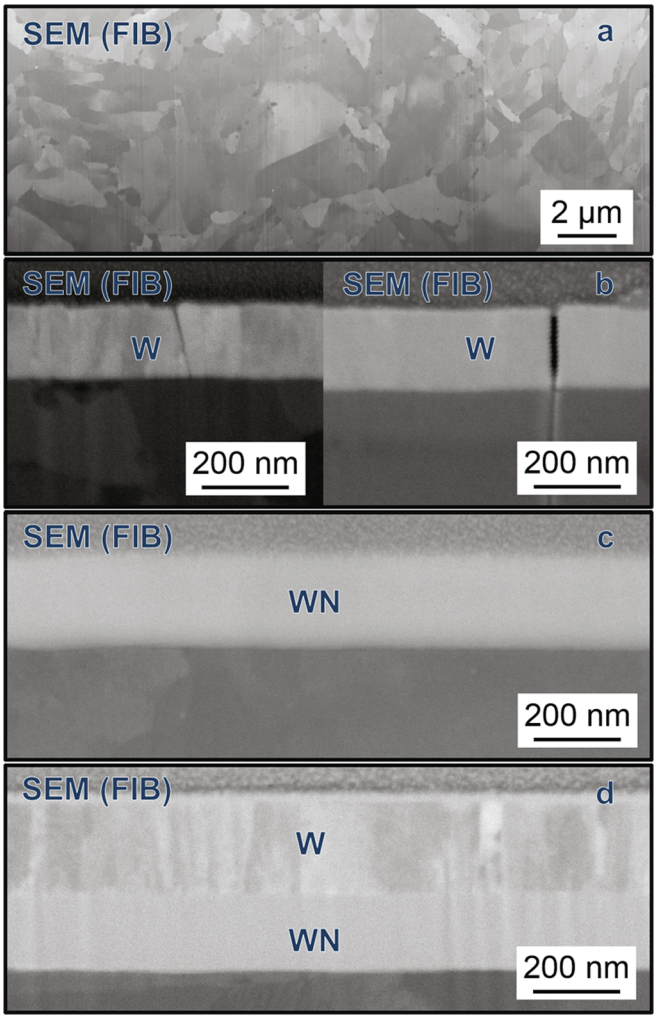

Fig. 1. SEM Figures on cross-sections prepared by FIB. a) for the Eurofer97 substrate; b) for the Eu97_W sample: left after annealing, right: after permeation measurement; c) for the Eu97_WN sample after annealing; d) for the Eu97_WNW sample after annealing. Please note the different magnification in Figure a).

By measuring the permeation flux as a function of the applied deuterium pressure, the limiting process can be determined. In the diffusion limited regime, the permeation flux is proportional the square root of the applied deuterium pressure. If the processes at the surface or interface are slow and therefore the determining processes, the permeation flux is linear dependent to applied pressure.

4. Results

In Fig. 1 a-d the SEM figures on cross sections prepared by FIB are shown. In Fig. 1a) the microstructure of the bare Eurofer97 sample can be observed. In b) the tungsten coated substrate is shown. Already after annealing, there are cracks in the tungsten layer due to the very different thermal expansion coefficients of tungsten and steel ($4{\cdot}10^{-6}$ 1/K and $12{\cdot}10^{-6}$ 1/K, respectively). After the permeation measurement, the cracks propagate, as can be seen in the right part of Fig. 1b). The SEM on Eu97_WN is shown in Fig. 1c. A smooth and dense layer without cracks is visible after annealing. In Fig. 1d) the SEM of the Eu97_WNW layer is shown. The microstructures of the WN and the W are similar in this sandwich sample as it is in the coatings of the Eu97_W and Eu97_WN samples, but no cracks can be observed after annealing in the

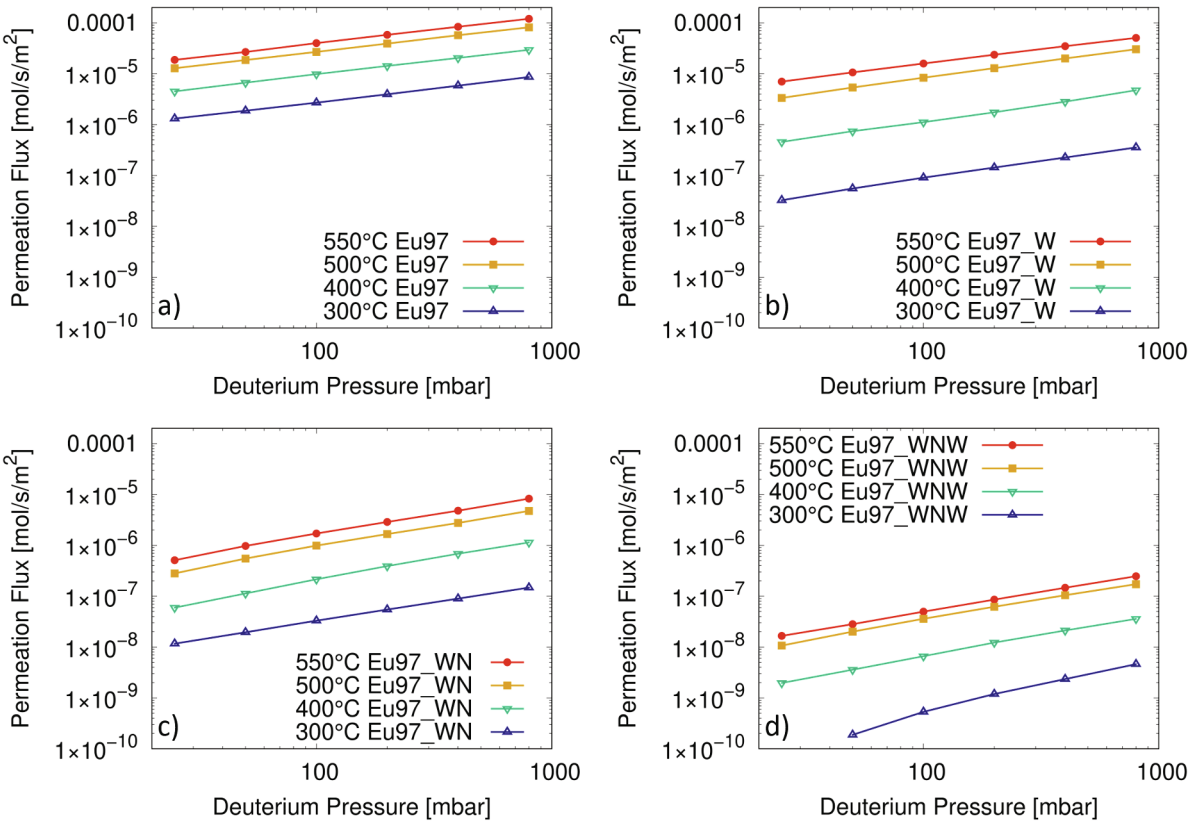

Fig. 2. Deuterium permeation flux versus the applied deuterium pressure at different sample temperatures (indicated by colors): a) for the Eurofer97 substrate (Eu97); b) for Eu97_W; c) for Eu97_WN; d) for Eu97_WNW. The sample thickness was in all cases 0.3 mm.

W layer. This indicates that the WN layer acts as a buffer between W and steel and compensating the stress due to the different thermal expansion coefficients of W and steel. The Eu97_WN and the Eu97_WNW samples were investigated after permeation measurement in the same way, but no change of microstructure or cracking of the layers was observed. From these measurements, the layer thicknesses were obtained: 180 nm W in the Eu97_W sample, 210 nm WN in the Eu97_WN sample and 170 nm WN and 220 nm W in the Eu97_WNW case.

The crystal structure of the layers were investigated by XRD and the diffraction patterns (not shown) confirm the tungsten α-phase for the tungsten layer and the WN phase for the WN layers. The composition of identically prepared WN layers was studied in detail in [6]. The crystal structures do not change after heat treatments and permeation measurements.

The permeation flux versus the applied deuterium pressure at different temperatures is shown in Fig. 2. From the pressure dependence, the limiting regime can be extracted. The exponent x of the pressure dependence p^x can be seen in Table 1. The bare substrate is in the diffusion limited regime, as expected for polished substrates, whereas the coated samples are in an intermediate regime with values between

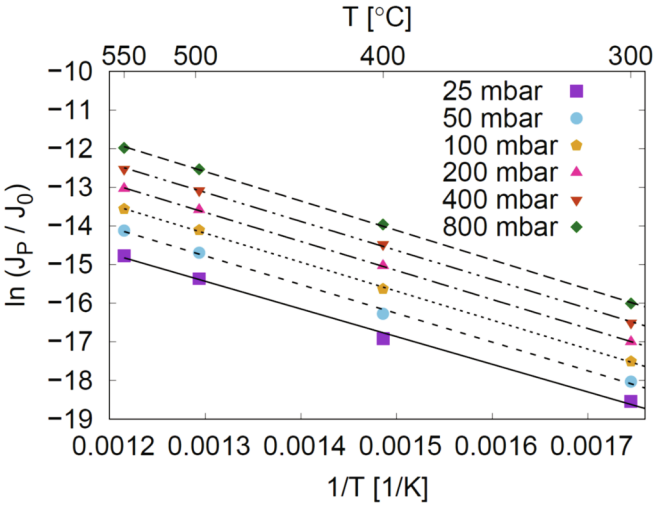

Fig. 3. Arrhenius plot for Eu97_WN with $J_0 = 1\frac{\text{mol}}{\text{m}^2\text{s}}$. The lines represent the fitted lines to the data in order to obtain E_P and P_0, see Table 1. The color points represent the measurement points at different deuterium pressures.

Table 1
The results obtained from temperature and pressure dependent permeation measurements (x, P_0, E_P) are calculated according to the equations given in part III.

Sample	p^x	$P_0\left[\frac{\text{mol}}{\text{ms}\sqrt{\text{mbar}}}\right]$	$E_P\left[\frac{\text{kJ}}{\text{mol}}\right]$
Eu97	0.5	$5.7(4)\cdot10^{-7}$	41.6(5)
Eu97_W	0.7	$8(1)\cdot10^{-5}$	82(2)
Eu97_WN	0.8	$5(3)\cdot10^{-7}$	62(1)
Eu97_WNW	0.8	$4(3)\cdot10^{-8}$	68(3)

$x = 0.7$ and $x = 0.8$. As explained above, the permeation activation energy and the constant can be obtained by an Arrhenius plot. As an example, the Arrhenius plot for the Eu97_WN sample is shown in Fig. 3. The Arrhenius equation is fulfilled for all samples, meaning that there is an exponential temperature dependence of the permeation process. The obtained values for the permeation activation energy (E_P) and constant (P_0) are shown in Table 1 and plotted in Fig. 4. Since the layered substrate samples are not in the diffusion-limited regime, but in an intermediate regime, the square root dependence of the applied pressure in Eq. (1) is not fulfilled. In order to compare the different layers, the

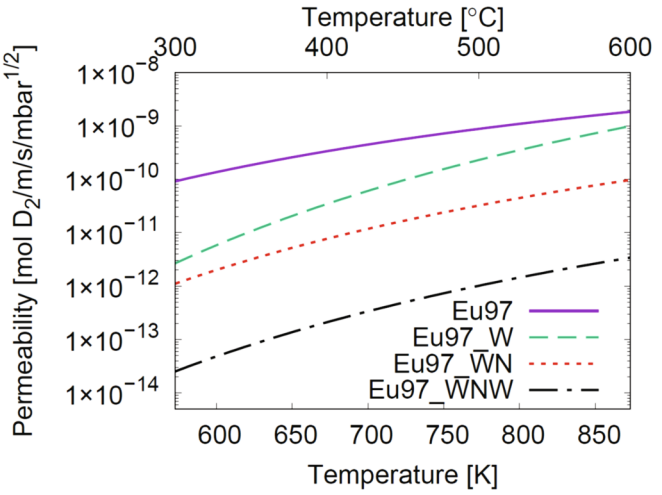

Fig. 4. The calculated permeability constant P_0 and activation energy E_P for the bare Eurofer97 (Eu97) substrate [8], the Eu97_W, the Eu97_WN and the Eu97_WNW samples, plotted with Eq. (2). These values are mean values of the different applied pressure data and valid in the measured temperature and pressure range only.

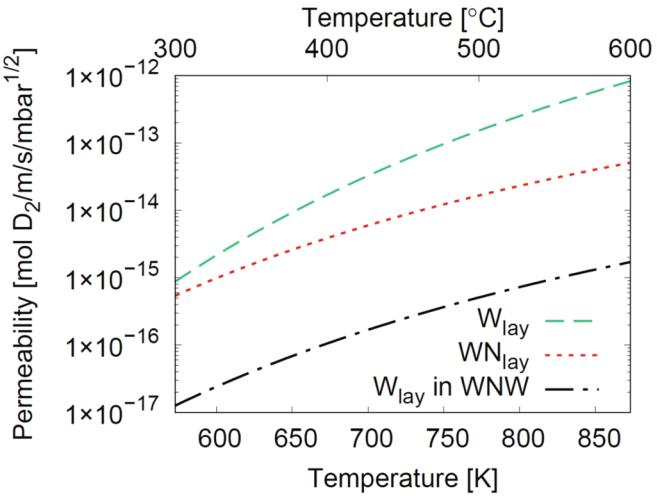

Fig. 5. The calculated layer permeabilities for W and WN layers for the Eu97_W and Eu97_WN samples and for the W layer in the Eu97_WNW sample, plotted with Eq. (2). The values can be found in Table 2.

square root dependence was assumed for all samples and the deviation from the square root dependence was considered in the error bars in Table 1. These values are valid in the applied pressure and sample temperature range only and the permeation constant is a mean value of the obtained values at different applied pressures.

The PRF values at 400 °C and 400 mbar are given in Table 2, in all cases for the total layered substrate compared to the bare Eu97 substrate. For a more reliable comparison of different TPB layers, the layer permeation can be estimated by Eq. (3) by using the values in Table 1 as explained above. The results are listed in Table 2. In case of the Eu97_W and Eu97_WN samples, the Eu_97 bare substrate permeability is used as P_{sub}. In order to estimate the influence of a tungsten top coating on the WN layered sample, the permeability of Eu97_WN is used as P_{sub} in the Eu97_WNW case. The temperature dependence of the layer permeabilities given in Table 2 is shown in Fig. 5.

5. Discussion

In Fig. 1a the SEM figure on a cross section of the Eu97_W sample is shown after annealing. In the W layer (light grey) a crack is observed. These cracks propagate during permeation measurement and the amount and width of the cracks increase, as can be seen in Fig. 1b. From the comparison of the permeation flux measurements through the substrate sample in Fig. 2a and through the W coated sample Eu97_W in Fig. 2b it is concluded that the permeation flux is only slightly reduced. The PRF value is only 8 at 400 °C and 400 mbar, see Table 2. Since the layer degrade during permeation measurements and the permeation flux increases, the conclusion is that these cracks act as shortcuts to the substrate. The layer would degrade even more, if the annealing or permeation measurement time increased, due to further crack propagation.

Table 2
The PRF of the total layered substrate compared to the bare Eu97 substrate at 400 °C and 400 mbar. The estimated layer permeability constant $P_{0,lay}$ and activation energy $E_{P,lay}$ for the W in the Eu97_W sample, the WN in the Eu97_WN sample and for the W in the Eu97_WNW sample, as calculated by Eq. (3).

Layer	PRF	$P_{0,lay}\left[\frac{\text{mol}}{\text{ms}\sqrt{\text{mbar}}}\right]$	$E_{P,lay}\left[\frac{\text{kJ}}{\text{mol}}\right]$
W	8	$4{\cdot}10^{-7}$	95
WN	31	$3{\cdot}10^{-10}$	63
W in WNW	1000	$2{\cdot}10^{-11}$	68

The WN layer in the Eu97_WN sample shows a very smooth and dense microstructure. There is no degradation of the layer during annealing and permeation measurement and the permeation measurement was very stable, see Fig. 2c. The permeation flux was reduced by one order of magnitude by this 210 nm thick layer. By using the calculated layer permeability, the permeation reduction of a 2 μm thick WN coating, which is a typical assumed thickness for a TPB coating in a fusion device, can be estimated. In Fig. 6 the permeation flux of a 2 μm coated WN Eu97 substrate with a substrate thickness of 0.5 cm is shown in comparison to an uncoated substrate of the same thickness at a applied deuterium pressure of 400 mbar. The permeation reduction is about two orders of magnitude. This example demonstrates that the PRF values is strongly dependent on the permeability and thickness of the used substrate and the thickness of the coating. Furthermore, the estimation of the permeation flux through a component in a fusion device is enabled by the layer permeability calculation.

For Eu97_WNW, no degradation of the coatings is observed and a

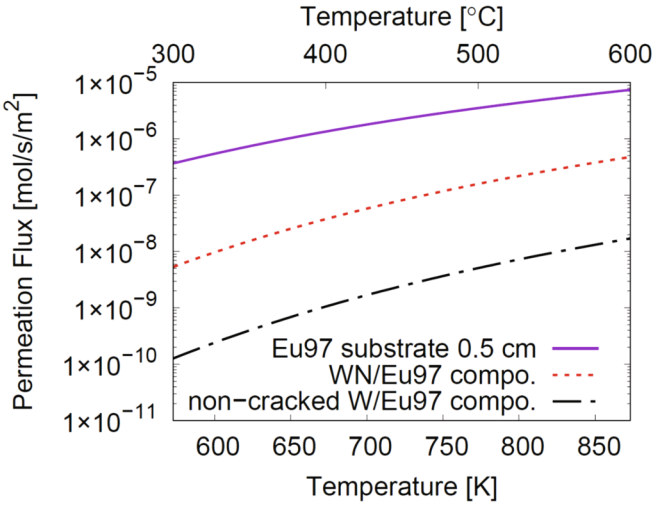

Fig. 6. The estimated permeation flux at an applied deuterium pressure of 400 mbar through a Eu97 substrate with a thickness of 0.5 cm, and through components with a TPB coating thickness of 2 μm and a Eu97 substrate thickness of 0.5 cm.

stable permeation measurement was obtained, see Fig. 2d. The PRF of this multi-layered system is 1000. From the calculation of the W layer permeability, one can conclude that this high PRF is mainly due to the non-cracked W layer. In comparison to WN, the permeability is two orders of magnitude smaller. In Fig. 6 the estimated permeation flux at 400 mbar for a non-cracked W layer with a thickness of 2 μm on a Eu97 substrate with a thickness of 0.5 cm is shown. The permeation reduction of this layer is nearly four orders of magnitude.

One has to note that in this calculated layer permeability the influence of the interface is included. In order to separate the influence of the interface and the bulk on the permeability, samples with different coating thicknesses have to be investigated. Furthermore, since the permeation process in the coated samples is limited not by diffusion only, but in an intermediate regime, the permeation reduction in a sandwich structure with different top coatings will be studied in the future.

6. Conclusions

The microstructure and the deuterium permeation was studied on three different W and WN coated Eu97 substrates. Due to the very different thermal expansion coefficient of W and martensitic steels, W coatings crack under thermal annealing and the use as TPB on steels is restricted. Even thin (below 200 nm) layers crack, the cracks act as shortcuts for the gas to the substrate and the permeation reduction is small. During permeation measurements, the W layer degraded further. In opposite to pure W coatings, WN and WNW coatings do not degrade under thermal annealing and are very suitable as TPB on steel. By calculating the layer permeability, which is independent of the thickness of the layer and the substrate, a reliable comparison between different TPB coating is possible compared to the comparison via the PRF values. A non-cracked W layer shows a two orders of magnitude smaller permeability as a WN layer in the applied pressure and sample temperature range. Furthermore, the permeation flux through a full component for a fusion device can be estimated by the layer permeability. A 2 μm WN layer can reduce the permeation flux through a 0.5 cm thick Eu97 substrate by about two orders of magnitude and a 2 μm non-cracked W layer can reduce the permeation flux by nearly four orders of magnitude. Samples with different top coatings and varying coating thicknesses will be studied in the future in order to investigate the influence of the interface on the deuterium permeation.

CRediT authorship contribution statement

A. Houben: Conceptualization, Methodology, Formal analysis, Investigation, Writing - original draft, Visualization. **M. Rasiński:** Investigation, Formal analysis. **L. Gao:** Investigation, Resources. **Ch. Linsmeier:** Conceptualization, Resources, Writing - review & editing, Funding acquisition.

Declaration of Competing Interest

The authors declare that they have no known competing financial interests or personal relationships that could have appeared to influence the work reported in this paper.

Acknowledgements

The authors thank B. Göths for substrate preparation. A part of this work has been carried out within the framework of the EUROfusion Consortium (WP PFC) and has received funding from the Euratom research and training program 2014–2018 and 2019–2020 under grant agreement No 633053. The views and options expressed herein do not necessarily reflect those of the European Commission.

References

[1] R. Causey, R. Karnesky, C.S. Marchi, in: R.J. Konings, (Ed.), Comprehensive Nuclear Materials, Elsevier, Oxford, 2012, pp. 511–549.
[2] J. Engels, A. Houben, P. Hansen, M. Rasinski, Ch. Linsmeier, Int. J. Hydrogen Energy 43 (2018) 22976.
[3] A. Kallenbach, R. Dux, M. Mayer, R. Neu, T. Pütterich, V. Bobkov, J. Fuchs, T. Eich, L. Giannone, O. Gruber, A. Herrmann, L. Horton, C. Maggi, H. Meister, H. Müller, V. Rohde, A. Sips, A. Stbler, J.S., Nucl. Fusion 49 (2009) 045007.
[4] M. Oberkofler, D. Douai, S. Brezinsek, J. Coenen, T. Dittmar, A. Drenik, S. Romanelli, E. Joffrin, K. McCormick, M. Brix, G. Calabro, M. Clever, C. Giroud, U. Kruezi, K. Lawson, C. Linsmeier, A.M. Rojo, A. Meigs, S. Marsen, R. Neu, M. Reinelt, B. Sieglin, G. Sips, M. Stamp, F. Tabares, J. Nucl. Mater. 438 (2013) S258, proceedings of the 20th International Conference on Plasma-Surface Interactions in Controlled Fusion Devices.
[5] K. Schmid, A. Manhard, Ch. Linsmeier, A. Wiltner, T. Schwarz-Selinger, W. Jacob, S. Maendl, Nucl. Fusion 50 (2010) 025006.
[6] L. Gao, W. Jacob, T. Schwarz-Selinger, A. Manhard, J. Nucl. Mater. 451 (2014) 352.
[7] L. Gao, W. Jacob, G. Meisl, T. Schwarz-Selinger, T. Hschen, U. von Toussaint, T. Dürbeck, Nucl. Fusion 56 (2015) 016004.
[8] A. Houben, J. Engels, M. Rasinski, Ch. Linsmeier, Nucl. Mater. Energy 19 (2019) 55.
[9] J. Engels, A. Houben, M. Rasinski, Ch. Linsmeier, Fusion Eng. Des. 124 (2017) 1140.
[10] A. Houben, M. Rasinski, Ch. Linsmeier, Plasma Fusion Res. 15 (2020) 2405016.